COBEM 2021 26th International Congress of Mechanical Engineering
November 22-26, 2021, Virtual Congress, Brazil

COB-2021-0723
PREDICTION OF HYPERSONIC REACTIVE FLOWS DURING ATMOSPHERIC ENTRY PROCEDURE OF THE FIRE II SPACE CAPSULE

Farney Coutinho Moreira
Instituto Tecnológico de Aeronáutica, ITA, 12228-900, São José dos Campos, SP, Brazil
farney.coutinho@gmail.com

William Roberto Wolf
Universidade Estadual de Campinas, UNICAMP, 13083-860, Campinas, SP, Brazil
wolf@fem.unicamp.br

João Luiz F. Azevedo
Instituto de Aeronáutica e Espaço, DCTA/IAE, 12228-904, São José dos Campos, SP, Brazil
joaoluiz.azevedo@gmail.com

Abstract. *Numerical simulations of a mixture of oxigen and nitrogen are presented for the Fire II capsule under hypersonic flow conditions including thermodynamic nonequilibrium. Two models for chemical nonequilibrium and transport properties are tested and their results are compared to experimental data available in terms of convective heat flux. The finite volume method is used to solve the Navier-Stokes equations including Park's two-temperature model. Results are presented in terms of heat flux distribution over the capsule surface and good agreement is observed between simulations and experimental data. The shock wave topology and species dissociation profiles lead to changes with respect to thermal non-equilibrium, presented in terms of the translational-rotational and vibrational-electronic temperature modes. At the initial moment of the reentry path, where flow speed and altitude are high, there is complete dissociation of nitrogen, N_2, and oxygen, O_2, molecules. Under such conditions, it is also possible to observe the occurrence of thermodynamic non-equilibrium through the magnitude difference of the translational-rotational and vibrational-electronic temperature modes inside the shock layer forming upstream of the capsule.*

Keywords: *Hypersonic flow, thermodynamic non-equilibrium, heat transfer, chemical dissociation*

1. INTRODUCTION

The atmospheric reentry procedure has always been a topic of great interest and importance in space missions. Spacecraft normally perform reentry maneuvers at a very high speed reaching Mach numbers greater than 20. When starting the atmospheric reentry procedure at altitudes above 100 km, the spacecraft and the crew have not yet been subjected to large drag loads, since the atmosphere is extremely fine and the friction is practically nonexistent. As the altitude is reduced in the descent procedure, the atmosphere becomes denser. In these flight conditions, very complicated effects occur in the flow, such as chemical reactions including dissociation, recombination and ionization. If the reentry velocity and the altitude are high enough, these chemical reactions are in thermodynamic non-equilibrium, and high temperature shock layers are formed near the vehicle surface, leading to vibrational-translational excitation of molecules during chemical reactions.

In the present work, a comparative study of the heat transfer rate is carried out at the stagnation point on the surface of the capsule. Such study is performed at seven points along the vehicle's descend trajectory. In order to carry out this comparative study, the results obtained with the improved numerical tool used in this research, called LEMANS code, are considered, and these results are compared to the experimental results obtained for the FIRE II capsule. It is important to note that the numerical results presented here consider only the convective effects, whereas the experimental data include both the convective and radiative effects Johnston *et al.* (2008).

An overall view of the 3-D model is presented in Fig. 1(a), while Fig. 1(b) shows geometrical details of the capsule with the dimensions of the three thermal protections used in the experiment and in the numerical simulations carried out in the present work. The capsule maintains the first thermal protection, with radius $R_n = 934.70$ mm during the reentry procedure up to an approximate altitude of 60 km. At this point along the trajectory, this first thermal protection is ejected from the capsule, and the downward path continues with the second thermal protection, which has a radius $R_n = 805.00$ mm. At an approximate altitude of 45 km, the second thermal protection shield is also ejected from the capsule. The remaining portion of the downward trajectory is flown with the third thermal protection shield, which has a

radius $R_n = 702.00$ mm.

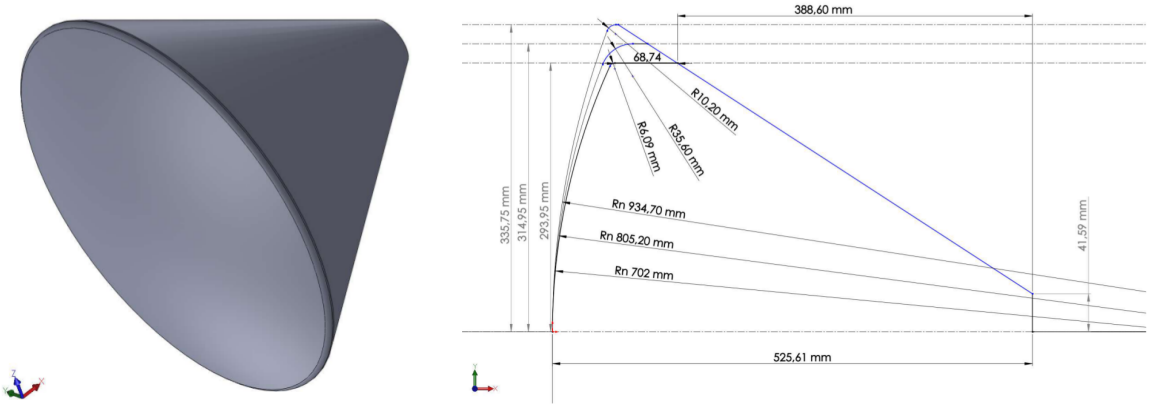

(a) 3D view of geometry (b) 2D view of geometry with dimensions

Figure 1. Fire II capsule model geometry.

Validation of simulation results for hypersonic flows is of paramount importance since uncertainties arise from numerical methods and models. In order to validate the present simulations, numerical results are compared to aerothermodynamic experimental data obtained from Ref. Cornette (1966). Computations are performed considering a gas mixture that simulates the atmosphere of planet Earth. The model considers a mass composition with 76.23% of molecular nitrogen, N_2, and with 23.77% of molecular oxygen, O_2. Results are presented in terms of heat flux distributions over the capsule surface as well as flow property behavior along the upstream stagnation line. An assessment in terms of flow topology and thermal analysis is presented focusing on thermodynamic non-equilibrium effects arising due to dissociation of the gas mixtures.

2. THEORETICAL FORMULATION

2.1 General Considerations

During the atmospheric reentry procedure, the vehicle is subjected to distinct flow regimes that vary as a function of the gas density and, thus, that depend on the altitude in the atmosphere. In the last phase of reentry, where density is sufficiently high, no-slip occurs on the vehicle surface. This behavior leads to shear stresses as defined for the flow in a continuous medium. The dimensionless parameter that defines the flow as continuum or rarefied is the Knudsen number, which can be written as

$$K_n = \frac{\lambda}{L} \, . \tag{1}$$

In this expression, the characteristic length scale, L, is a representative measure of the dimension of the fluid-immersed object. For the specific case of a reentry capsule, the outer diameter, or the outer radius, is typically used. The λ parameter is defined as the mean free path, *i.e.*, the average distance traveled by a fluid molecule between successive collisions. Through some mathematical manipulations, it is possible to rewrite the Knudsen number as a function of the Mach and Reynolds numbers Alladadi *et al.* (2013) as

$$K_n = \sqrt{\gamma \frac{\pi}{2}} \, \frac{M}{Re} \, . \tag{2}$$

Here, γ represents the ratio of specific heats, M is the Mach number and Re is the Reynolds number. The flow is considered continuum for Knudsen numbers up to $K_n = 0.1$. In this flow regime, the physical problem can be mathematically modeled by the Navier-Stokes equations. The so-called transition regime typically occurs with a Knudsen number ranging from $0.1 < K_n < 10$, and this type of flow should be solved through the kinetic theory of gases, mathematically described by the Burnett equation Agarwal *et al.* (2001). For Knudsen numbers $K_n > 10$, the flow becomes rarefied, also called free molecular flow, and statistical approaches that take into account binary collision models are required. The most widely used method for treating phenomena that occur in this last flow regime is the Direct Simulation Monte Carlo (DSMC) method Bird (1994).

In the simulations addressed in the present work, the flows are modeled as continuum since we expect the Knudsen numbers to be of order 10^{-3}. Hence, the Navier-Stokes equations constitute an accurate model for the present high-enthalpy continuum flows. These equations are solved using Park's two-temperature model to account for thermodynamic non-equilibrium and weak ionization effects Park (1988). Hence, it is assumed that the rotational and translational energy modes of all species can be described by a single temperature, T_{tr}, and that the vibrational energy mode of all species plus the electron energy can also be described by a single temperature, T_{ve} Scalabrin (2007); Martin *et al.* (2012).

2.2 Conservation Equations and Related Models

Through the Boltzmann equation and the Chapman-Enskog theory Bobylev (1982), it is possible to obtain the system of conservation equations for transport of mass, momentum and energy, which are herein referred to as the Navier-Stokes equations. Here, this system of conservation equations contains a source term that represents chemical reactions including dissociation and ionization under thermodynamic non-equilibrium. A second source term appears because the present approach takes advantage of the axisymmetry of the configuration and, hence, treats the flows of interest as axisymmetric flows. The equations can be written in multi-dimensional form using index notation as follows

$$\frac{\partial Q}{\partial t} + \frac{\partial (F_j - F_{v_j})}{\partial x_j} = S_{cv} + S_{axi} \,, \tag{3}$$

where Q represents the vector of conserved variables and it is defined as

$$Q = \left\{ \begin{array}{ccccccc} \rho_1 & \dots & \rho_N & \rho u_i & E & E_{ve} \end{array} \right\}^T . \tag{4}$$

In the previous equations, index notation has been used and repeated indices imply summation while a free index represents a vectorial equation. In the vector of conserved variables, the terms ρ_1, ..., ρ_N represent the densities of the N chemical species present in the gas mixture. The macroscopic flow velocity components are represented by u_i, the total energy per unit volume is described by E, and the electronic vibrational energy per unit volume of the mixture is represented by E_{ve}.

The components in the j-th direction of the inviscid, F_j, and viscous, F_{v_j}, flux terms are defined as

$$F_j = \left\{ \begin{array}{c} \rho_1 u_j \\ \vdots \\ \rho_N u_j \\ \rho u_i u_j + p\delta_{ij} \\ (E+p)u_j \\ E_{ve} u_j \end{array} \right\} \quad \text{and} \quad F_{v_j} = \left\{ \begin{array}{c} -J_{1,j} \\ \vdots \\ -J_{N,j} \\ \tau_{ij} \\ \tau_{ij} u_i - (q_{tr,j} + q_{ve,j}) - \sum (J_{s,j} h_s) \\ -q_{ve,j} - \sum (J_{s,j} e_{ve,s}) \end{array} \right\} . \tag{5}$$

In the above equations, the p variable represents the mixture pressure and δ_{ij} is the Kronecker delta. According to Fick's law, the diffusion flux of the s-th chemical species in the j-th direction is represented by $J_{s,j} = \rho D_s \frac{\partial Y_s}{\partial x_j}$, and the viscous stress tensor components are defined by τ_{ij}. Here, D_s and Y_s represent the diffusion coefficient and molar fraction of species s, respectively. The thermal flux from translational-rotational energy in the j-th direction is given by $q_{tr,j}$ while $q_{ve,j}$ represents the thermal flux component from electronic-vibrational energy in the j-th direction. Moreover, h_s represents the enthalpy of the s-th chemical species.

The pressure is calculated assuming that each species can be modeled using an ideal gas relation and Dalton's law of partial pressures Gillespie (1930)

$$p = \sum_{s=1}^{N} \rho_s \frac{R}{M_s} T_{tr} + \rho_e \frac{R}{M_e} T_{ve} \,, \tag{6}$$

where R is the universal gas constant, T_{tr} is the temperature of translational and rotational modes, T_{ve} is the temperature of vibrational and electronic modes, ρ_s and M_s are the density and molecular weights of the individual chemical species, respectively, ρ_e is the electronic density and M_e is the electronic molecular weight.

The viscous stress tensor for a Newtonian fluid is defined as

$$\tau_{ij} = \mu \left(\frac{\partial u_i}{\partial x_j} + \frac{\partial u_j}{\partial x_i} \right) - \left(\frac{2}{3}\mu - \beta \right) \frac{\partial u_k}{\partial x_k} \delta_{ij} \,, \tag{7}$$

where μ is the shear viscosity and β is the bulk viscosity. Through Stokes' hypothesis, we assume that $\beta = 0$ Blottner *et al.* (1971); Nompelis *et al.* (2009). The bulk viscosity contributes to the dilatational term appearing in the normal stresses and arises from the exchange of momentum between colliding molecules and their internal degrees of freedom. Therefore, one

could expect that the momentum exchange across the strong shock waves observed in the present calculation procedure could be directly impacted by this parameter, especially if flows containing carbon dioxide were to be considered. Recent estimation models of bulk viscosity for ideal gases under different temperature ranges are provided in Ref. Cramer (2012); Sharma and Kumar (2019). In general, these models are designed for lower temperatures than those found in the present flows. Moreover, since this is still a topic of investigation, Stokes' hypothesis is assumed in the present work in order to avoid inaccuracies in the evaluation of the bulk viscosity and because we are primarily concerned with reentry to the Earth atmosphere in the present case.

The heat fluxes are modeled according to Fourier's law of heat conduction as

$$q_{tr,j} = -k_{tr}\frac{\partial T_{tr}}{\partial x_j} \qquad \text{and} \qquad q_{ve,j} = -k_{ve}\frac{\partial T_{ve}}{\partial x_j} \, . \tag{8}$$

The thermal conductivity of the mixture for each energy mode is calculated using the approach proposed by Eucken Vincenti and Kruger (1982). Hence, the conductivity of the translational-rotational and vibrational-electronic modes are computed, respectively, as

$$k_{tr,s} = \frac{5}{2}\mu_s Cv_{tr,s} + \mu_s Cv_{ve,s} \tag{9}$$

and

$$k_{ve,s} = \mu_s Cv_{ve,s} \, . \tag{10}$$

Here, $Cv_{tr,s}$ is the constant volume specific heat related to translational-rotational temperature and $Cv_{ve,s}$ is the constant volume specific heat related to vibrational-electronic temperature for the s-th chemical species. The mixture transport properties are modeled using Wilke's semi-empirical mixing rule Wilke (1950) as

$$\mu = \sum_s \frac{Y_s \mu_s}{\phi_s} \, , \tag{11}$$

and

$$k = \sum_s \frac{Y_s k_s}{\phi_s} \, , \tag{12}$$

The μ_s and k_s parameters represent the dynamic viscosity and thermal conductivity coefficients for the individual s-th species. The ϕ_s term is calculated using

$$\phi_s = \sum_r Y_r \frac{\left[1 + \sqrt{\frac{\mu_s}{\mu_r}}\left(\frac{M_r}{M_s}\right)^{1/4}\right]^2}{\sqrt{8\left(1 + \frac{M_s}{M_r}\right)}} \, . \tag{13}$$

In the equation above, μ_r and M_r are the viscosity coefficient and molecular weight, respectively, of species r involved in the binary collision with species s. These values can be found in Ref. Scalabrin (2007).

The S_{axi} source term represents the additional surface stresses that appear from the axisymmetric formulation. This term adds a contribution only to the y-momentum equation in order to counterbalance the pressure and viscous forces acting on the side surfaces of the control volume. Hence, S_{axi} is given by

$$S_{axi} = \left\{ \begin{array}{ccccccc} 0 & \ldots & 0 & \left[-p + 2\mu\left(\frac{u_2}{\bar{x}_2} - \frac{1}{3}\frac{\partial u_k}{\partial x_k}\right)\right]\frac{\delta_{i2}}{\bar{x}_2} & 0 & 0 \end{array} \right\}^T \, . \tag{14}$$

In the equation above, the $\bar{x}_2$ term is the radial coordinate measured from the axis of symmetry to the cell centroid. One should remember that, for an axisymmetric flow, the dilatation term is given by $\dfrac{\partial u_k}{\partial x_k} = \dfrac{\partial u_1}{\partial x_1} + \dfrac{\partial u_2}{\partial x_2} + \dfrac{u_2}{\bar{x}_2}$, where x_1 and x_2 are the axial and radial directions, respectively.

In Eq. (3), the S_{cv} source term represents the rates of mass production of species during chemical reactions. This term can be written as

$$S_{cv} = \left\{ \begin{array}{cccccccc} \dot{\omega}_1 & \ldots & \dot{\omega}_N & 0 & 0 & 0 & 0 & \dot{\omega}_v \end{array} \right\}^T \, , \tag{15}$$

where $\dot{\omega}_v$ is the vibrational energy source term, and $\dot{\omega}_1$, ..., $\dot{\omega}_N$ represent, respectively, the mass production rates of all N species due to the chemical reactions.

2.3 Chemical Species

Phenomena associated with dissociation and ionization caused by high-enthalpy flows, typically encountered in hypersonic conditions and atmospheric entry, will determine the chemical species present in the mixture. Some chemical models have been developed and are used to represent these phenomena according to the complexity of the flow physics involved and their chemical reactions Gnoffo *et al.* (1989). The information in Table 1 indicates the chemical species that are included in the two chemical species models used for the present simulations. The models are referred to as the 5-species and 11-species models in the paper and they are typical descriptions of air composition for reentry simulations on the Earth atmosphere.

Table 1. Chemical species models for Earth atmosphere (air) used in the present work.

MODEL (NUMBER OF SPECIES)	SPECIES
5	N_2, O_2, NO, N, O
11	N_2, O_2, NO, N, O, N_2^+, O_2^+,NO^+,N^+, O^+, e^-

2.4 Model of Chemical Reactions

For all previous models, the chemical reactions of dissociation and ionization can be represented by the following equation

$$\sum \alpha_{rs} \rightleftharpoons \sum \beta_{rs} \quad . \tag{16}$$

Here, s represents the chemical species, and α_{rs} and β_{rs} are the stoichiometric coefficients of the reagents and products, respectively. The reactions are written such that the right arrow represents an endothermic reaction. The rate of chemical production of the s-th species is given by

$$\dot{\omega}_s = M_s \sum_{r=1}^{nr} (\beta_{rs} - \alpha_{rs}) \left[k_{fr} \prod_{s=1}^{N} \left(\frac{\rho_s}{M_s} \right)^{\alpha_{rs}} - k_{br} \prod_{s=1}^{N} \left(\frac{\rho_s}{M_s} \right)^{\beta_{rs}} \right] \quad , \tag{17}$$

where k_{fr} and k_{br} are the forward and backward reaction rates. The latter depends on the equilibrium constant Park (1993), k_{eq}, as

$$k_{br} = \frac{k_{fr}\left(T_c\right)}{k_{eq}\left(T_c\right)} \quad , \tag{18}$$

where the values of $k_{eq}\left(T_c\right)$ are obtained by curve fits as follows

$$k_{eq} = \exp\left[A_1 \left(\frac{T_c}{10^4} \right) + A_2 + A_3 \ln\left(\frac{10^4}{T_c} \right) + A_4 \left(\frac{10^4}{T_c} \right) + A_5 \left(\frac{10^4}{T_c} \right)^2 \right] \quad . \tag{19}$$

The A_1, A_2, A_3, A_4 and A_5 coefficients are functions of the flow particle number density within the range of the data tabulated in Ref. Park (1989). For number densities outside the range available, the tabulated values for the maximum and minimum number densities are used accordingly.

Under conditions of chemical non-equilibrium, it is reasonable to assume that the order of magnitude of flow and chemical reaction characteristic timescales are comparable. Thus, models that consider a finite rate of chemical reactions are appropriate to consider non-equilibrium effects. The two-temperature model proposed by Park Park (1989) is widely used due to its simplicity. This model includes the effects of chemical non-equilibrium in the calculations of dissociation rates using a control temperature, T_c, according to

$$T_c = T_{tr}^a T_{ve}^b \, . \tag{20}$$

In this equation, T_{tr} is the temperature from the translational-rotational modes and T_{ve} is the temperature due to the excitation of the vibrational-electronic modes. Constants a and b define the non-equilibrium weight factor that controls the energy transfer between dissociation and ionization reactions. The dissociation reactions are controlled by a combination of the translational-rotational and vibrational-electronic temperatures to account for the fact that vibrationally excited molecules are more likely to dissociate Park (1988).

Niu *et al.* Niu *et al.* (2018) present a thorough analysis in terms of the non-equilibrium weight factor considering $a = b = 0.5$, and $a = 0.7$ and $b = 0.3$, for different chemical models. It is shown that the weight factor has an important role on the distribution of the vibrational-electronic temperature in the non-equilibrium process. Here, we use the standard values $a = b = 0.5$. The previous reference shows that this selection leads to good comparisons with experimental results obtained for a blunt body flow in terms of spectral intensity. Moreover, we also performed simulations with $a = 0.7$ and $b = 0.3$ for the present CO_2 flows, obtaining similar results.

In Eq. 17, the forward reaction rates are calculated using Arrhenius curve fits as

$$k_{fr} = A\, T_c^{\eta_k} \exp\left(-\frac{\theta_r}{T_c}\right) \quad , \tag{21}$$

where A is the pre-exponential factor, η_k is the temperature dependence, and θ_r is the activation energy. The forward chemical kinetic rate coefficients used in this work are those proposed by Park Park (1993).

3. NUMERICAL FORMULATION

The Navier-Stokes equations are solved using the LeMANS parallel code developed at University of Michigan Scalabrin (2007); Martin *et al.* (2012). The solver employs the finite volume method with a cell-centered approach. In this work, axisymmetric flows are computed using meshes solely composed of quadrilaterals in order to better resolve the boundary layers and shock waves present in hypersonic flows.

The inviscid fluxes across cell faces are discretized using a modified version of the Steger-Warming flux vector splitting scheme MacCormack and Candler (1989) which is less dissipative and yields better results along boundary layers. The method switches to the original Steger-Warming scheme Steger and Warming (1981) at shock waves by using a pressure switch. A second-order reconstruction of the inviscid fluxes is implemented as discussed in Ref. Scalabrin (2007). The viscous fluxes are calculated using a second-order centered scheme that combines properties at cell centers and at the nodes. The property values at the nodes are calculated using a simple average of the cell values that share the node. The use of this method increases the stencil employed in the derivative calculations in order to avoid loss of accuracy when using unstructured meshes. No-slip velocity boundary conditions with catalytic or non-catalytic isothermal walls are applied along the solid surfaces for the calculations discussed in the present work.

The spatial discretization of the source term is the same as that used to calculate the viscous flux terms. The values of properties on the left and right sides of a volume face are obtained using the values on the centroid of the respective volume and also the values of properties on the nodes that make up the control volume Jawahar and Kamath (2000). Forward and backward chemical reaction rates can achieve large values depending on the control volume temperature, especially for low equilibrium constant values, k_{eq} Park (1988). Another numerical problem associated with the source term of chemical reactions is related to the density of chemical species, which needs to be positive. Negative values of densities of chemical species cause the source terms to change sign, which leads to numerical instabilities. The problem arises from the fact that, during the convergence process, and since some of those densities, at a given control volume, can be very small, the calculation procedure might yield negative values to the density of some species. In order to overcome any problems in the calculation of source terms, chemical reaction rates are numerically obtained using a modified temperature as discussed in Ref. Scalabrin (2007).

Numerical instabilities may also appear with the use of explicit methods for time integration of the Navier-Stokes equations including source terms with chemical reactions. In such cases, the time step restriction arising from numerical stiffness does not allow an acceptable iteration time for achieving solution convergence Hirsch (2007). Since we sought steady state flow solutions, an alternative to avoid this type of problem is to use implicit schemes for time integration of the equations. This approach improves efficiency and robustness, allowing larger time steps while avoiding the growth of numerical instabilities. In this work, the time integration is performed using a line implicit method Venkatakrishnan (1995).

4. RESULTS

In this section, results of hypersonic flow calculations are presented modeling the atmospheres of planet Earth. In order to validate the numerical model, the heat flow at the stagnation point in the frontal region of the FIRE II capsule is calculated. The numerical results are compared with experimental flight data, according to the conditions presented in Table 2. In the table, $T(s)$ describes the time in seconds of the experiment counted from the launch from the ground, $H(km)$ represents the flight altitude, ρ_∞ is the freestream density of the flow, T_∞ is the freestream temperature, T_w is the temperature of the surface of the capsule, U_∞ is the flow speed, R_n represents the frontal radius of the thermal protections in each phase of the flight, M_∞ is the freestream Mach number, Re_∞ is the reference Reynolds number and Kn_∞ is the freestream Knudsen number of the flow.

Table 2. Flow configurations investigated in the present work.

$T(s)$	$H(km)$	$\rho_\infty(kg/m^3)$	$T_\infty(K)$	$T_w(K)$	$U_\infty(m/s)$	$R_n(m)$	M_∞	Re_∞	Kn_∞
1634	76.42	3.72×10^{-5}	195	615	11,360	0.935	40.50	1.01×10^4	5.93×10^{-3}
1636	71.02	8.57×10^{-5}	210	810	11,310	0.935	38.85	2.19×10^4	2.63×10^{-3}
1637	67.05	1.47×10^{-4}	228	1,030	11,250	0.935	37.09	3.50×10^4	1.57×10^{-3}
1640	59.62	3.86×10^{-4}	254	1,560	10,970	0.935	34.27	7.99×10^4	6.35×10^{-4}
1643	53.04	7.80×10^{-4}	276	640	10,480	0.805	31.40	1.38×10^5	3.37×10^{-4}
1645	48.37	1.32×10^{-3}	285	1,520	9,830	0.805	28.99	2.17×10^5	1.97×10^{-4}
1648	41.60	3.25×10^{-3}	267	503	8,100	0.702	24.68	4.32×10^5	8.46×10^{-5}

4.1 Grid Convergence Study

Numerical simulations are performed using 128 Intel Xeon E5-2680v2 2.8 GHz cores. The grids used in the simulations are composed exclusively of quadrilaterals to better resolve the shock waves and boundary layers in the present flows and to improve the quality of results along the vehicle surface. As previously discussed, actually, the FIRE II capsule has three distinct configurations with different outer shell diameters, due to the use of heat shields which are used and ejected during the reentry flight. These three different configurations have been described in Fig. 1(b). The heat flow calculations are very sensitive to the size of the mesh cells close to the wall. According to recommendations in the literature Moreira *et al.* (2021), for the present flow conditions, the cell Reynolds number, Re_{cell}, must be kept below 3.0 for the best capture of the heat flow at the surface. A mesh refinement study analyzing the number of volumes and the size of the first mesh cell in the wall-normal direction, for each of the three distinct geometric configurations, is being carried out and will be available in the final version of the article. The medium mesh has 350 volumes in the longitudinal direction along the body, and 150 volumes in the wall-normal direction for each of the three configurations analyzed. Other two grids are being considered for each of the three configurations, namely, a course and a fine mesh. These meshes have 100 and 200 grid cells in the wall-normal direction, whereas the number of mesh cells is kept constant, and equal to 350 cells, in the longitudinal direction. A view of the medium meshes for the three configurations is presented in Fig. 2.

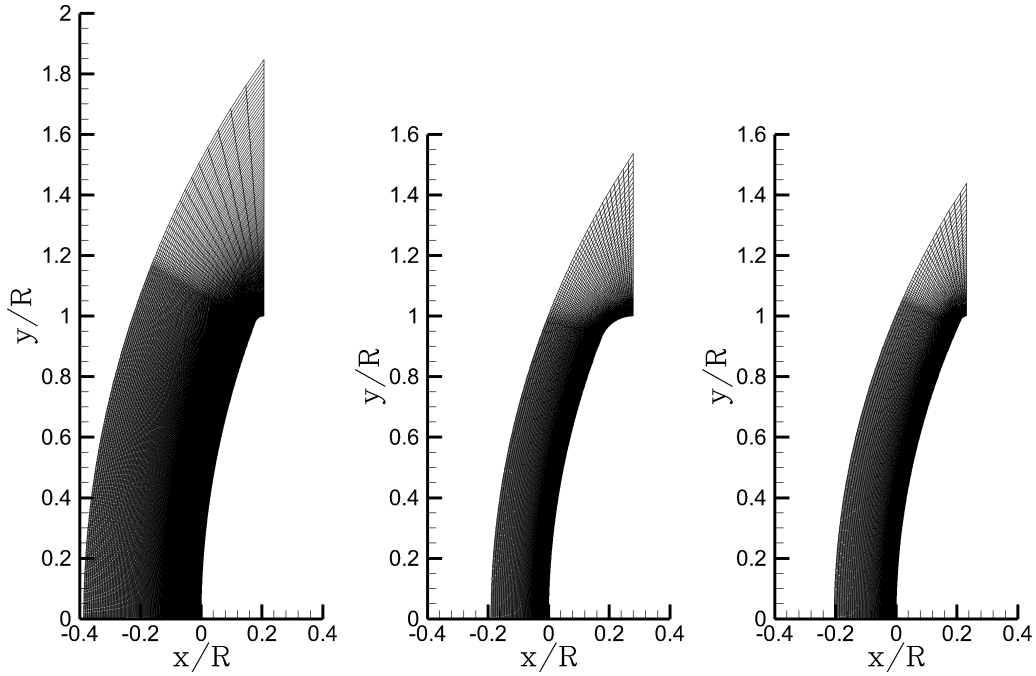

(a) Configuration 1 ($R_n = 0.935m$) (b) Configuration 2 ($R_n = 0.805m$) (c) Configuration 3 ($R_n = 0.702m$)

Figure 2. Medium computational grids used in the FIRE II numerical simulations.

Figure 3 shows a detail of Medium computational grid configuration 2 in the region close to the body surface. In this figure, it is possible to observe the refinement in the adjacent region of the capsule surface, necessary for the correct capture of the heat transfer rate on the vehicle surface.

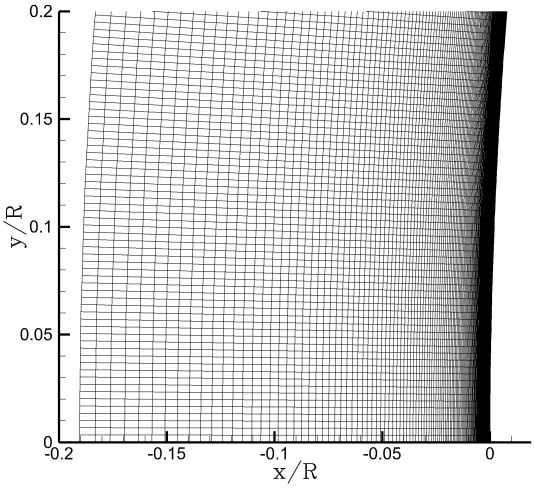

(a) Configuration 2 detail

Figure 3. Detail of the grid of configuration 2 in the region close to the body surface.

4.2 Convective Heat Transfer

In this section, results simulating reentry into the atmosphere of planet Earth are presented. Initially, an analysis of the influence of the chemical species models on the results obtained with catalytic and non-catalytic boundary conditions is carried out. Figure 4 presents the results for the heat flow at the stagnation point of the flow, comparing calculations performed with the 5-species and the 11-species models. The results obtined with the catalytic wall boundary conditions are shown in Fig. 4(a), whereas those obtained with the non-catalytic wall boundary conditions are presented in Fig. 4(b).

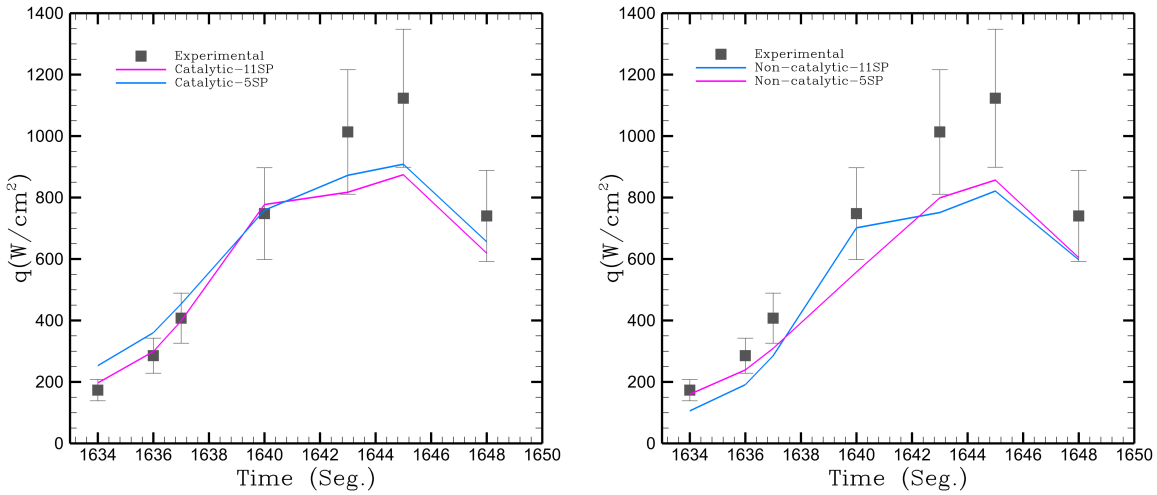

(a) Catalytic (b) Non-catalytic

Figure 4. Comparison of the heat flow with the 5-species and the 11-species models.

The results in Fig. 4(a) confirm an expected trend of increased temperature and, therefore, increased heat flow when using the 5-chemical species model. This increase in the heat flow occurs due to the absence of ionization chemical reactions in the 5-species model, making it impossible for the calculations to correctly capture the effects of the conversion of thermal energy used to carry out the ionization reactions. Hence, the corresponding reduction in the temperature for the flow inside the shock layer does not happen and the observed higher heat flow are the result. The same characteristics observed in the comparison of the heat flow for the two species models, when using catalytic walls, are also present in the calculations when using non-catalytic walls, as shown in Fig. 4(b).

Figure 5 presents some flow visualization, in terms of temperature contours, for the calculations over the initial thermal protection used by the capsule until $t = 1640$ seconds. As peviously discussed, at this instant along the flight, this initial thermal protection shield is ejected and the second thermal protection takes on the function of the vehicle protective

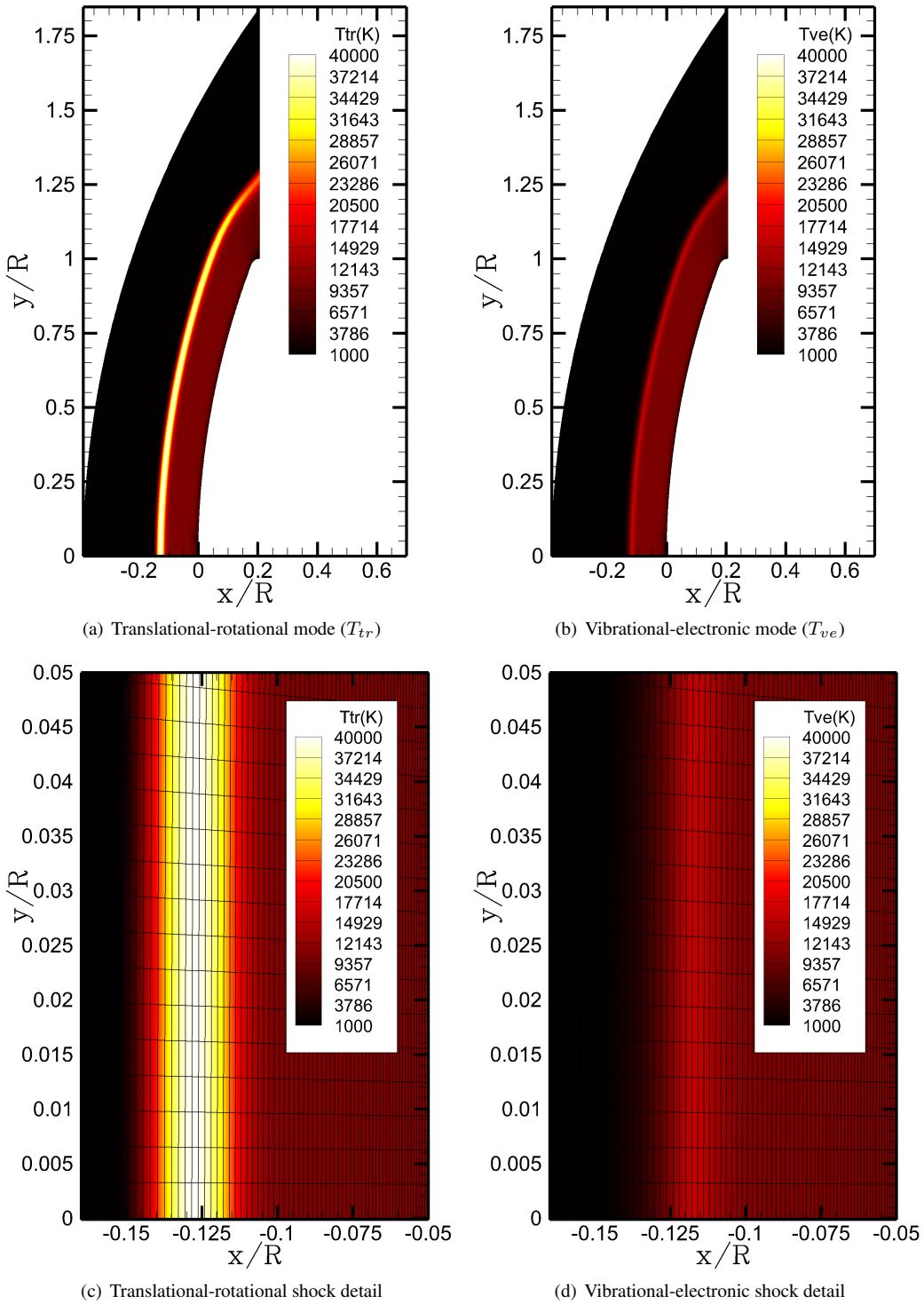

(a) Translational-rotational mode (T_{tr})

(b) Vibrational-electronic mode (T_{ve})

(c) Translational-rotational shock detail

(d) Vibrational-electronic shock detail

Figure 5. Temperature contours for the two temperature modes. Flight time $t = 1634$ seconds, catalytic wall boundary conditions, and the 11-species model are considered in the simulation.

shield. The results shown in the figure again consider the flight conditions at time $t = 1634$ seconds. Figures 5(a-c) and (b-d) show, respectively, the translational-rotational and the vibrational-electronic temperature modes for the flowfield at $t = 1634$ seconds, which is the beginning of the reentry trajectory, here studied, of the FIRE II capsule.

Figures 5(a) and (b) indicate that there is considerable difference in the maximum temperature reached in the two temperature modes. Hence, the translational-rotational mode is excited with greater intensity and it reaches the maximum temperature value of approximately 40,000 K, whereas the vibrational-electronic mode only reaches a maximum value of approximately 16,000 K. Such behavior is associated with the low density at this higher altitudes, $H = 76.42$ km,

coupled with the high kinetic energy due to the very high Mach number, $M_\infty = 40.50$, of the flow under these conditions. The occurrence of thermodynamic non-equilibrium can be visualized in the form of an arc approximately 19.35 mm thick which is detached in front of the surface of the vehicle.

Figures 5(c) and (d) show a detail of the frontal region close to the shock wave, including the detail of the computational mesh. The figure suggests the need for a mesh refinement in this region to better capture the high gradients of the translational-rotational mode of temperature. The authors are working on this refinement study, which will be available in future publications.

Good agreement of the numerical results with the experimental data has been observed for all test cases addressed so far. The results, that have been obtained up to the time of this writing, seem to demonstrate the effectiveness of the numerical tool in providing consistent and reliable engineering data, such as the heat flow distributions. It should be observed that the heat flow is an essential parameter for the adequate design of the thermal protection system for a reentry capsule. Therefore, simulations as the ones discussed in the present work are relevant for guaranteeing the survivor of the reentry phase of these capsules.

5. CONCLUSIONS

Hypersonic flows in thermodynamic non-equilibrium are investigated for gas mixtures that simulate the atmosphere of planet Earth. The Navier-Stokes equations are solved including source terms that model the chemical reactions occurring in the present high-enthalpy flows. A two-temperature model is applied to individually account for the translational and rotational modes, and the vibrational and electronic modes. The Earth atmosphere is considered to be composed of a mixture of oxygen and nitrogen. A grid refinement study is being conducted to identify the mesh requirements for convergence of results. Then, validation of numerical solutions, by comparing to experimental data, is shown in terms of stagnation point heat flow for different instants of the reentry path. The results obtained so far indicate good agreement of computed results with the experimental data.

The purpose of the present analysis is to obtain convective thermal flow data at the flow stagnation point and compare these numerical results with the experimental data available for convective and radiative fluxes on the surface of the capsule. It is important to note that, in the current implementation, the calculated heat flux contemplates only the convective portion, with the rate of heat transfer by radiation being the object of future studies.

Results demonstrate that, by applying the non-catalytic wall boundary conditions, there is a considerable mismatch between the numerical solutions and the experimental data. The wall heat flux, obtained with the non-catalytic wall boundary conditions, indicate a reduction in the magnitude of such heat flux when compared to the results obtained with the catalytic wall. This behavior occurs due to the absence of mass fraction variation in the normal direction of the wall, causing the flow to lose the condition of local thermodynamic equilibrium and, hence, changing the temperature profile on the vehicle surface.

In addition to the influence of the boundary conditions on the heat flux calculation, the authors also verify an increase in temperature, and consequently in the heat flux, when using the 5-species chemical model. This increase is justified by the absence of chemical ionization reactions, making it impossible to convert the thermal energy used in the ionization reactions that would result in a local temperature reduction inside the shock layer.

6. ACKNOWLEDGEMENTS

The authors gratefully acknowledge the support for the present research provided by Conselho Nacional de Desenvolvimento Científico e Tecnológico, CNPq, under the Research Grants No. 309985/2013-7, 304335/2018-5 and 407842/2018-7. The work is also supported by computational resources of the Center for Mathematical Sciences Applied to Industry (CeMEAI), funded by Fundação de Amparo à Pesquisa do Estado de São Paulo, FAPESP, under the Research Grant No. 2013/07375-0. The authors acknowledge the National Laboratory for Scientific Computing, LNCC/MCTI, Brazil, for providing HPC resources of the SDumont supercomputer, under the HFWBTF project, which have contributed to the research results reported in the present paper. FAPESP Research Grant No. 2013/08293-7 is further acknowledged by the authors. Support to the first author under the FAPESP Scholarship Grant No. 2021/02705-8 and additional support to the third author under FAPESP Research Grant No. 2013/07375-0 are also gratefully acknowledged.

7. REFERENCES

Agarwal, R.K., Yun, K.Y. and Balakrishnan, R., 2001. "Beyond Navier–Stokes: Burnett equations for flows in the continuum–transition regime". *Physics of Fluids*, Vol. 13, No. 10, pp. 3061–3085. doi:10.1063/1.1397256.

Alladadi, F.A., Rongier, I. and Wilde, P.D., 2013. *Safety Design for Space Operations*. Elsevier, Oxford.

Bird, G.A., 1994. *Molecular Gas Dynamics and the Direct Simulation of Gas Flows*. Oxford University Press, Oxford.

Blottner, F.G., Johnson, M. and Ellis, M., 1971. "Chemically reacting viscous flow program for multi-component gas mixtures". Technical report, Sandia Labs.

Bobylev, A.V., 1982. "The Chapman-Enskog and grad methods for solving the Boltzmann equation". In *Akademiia Nauk SSSR Doklady*. Vol. 262, pp. 71–75.

Cornette, E.S., 1966. "Forebody temperatures and calorimeter heating rates measured during project FIRE 2 reentry at 11.35 kilometers per second". Technical report, NASA-TM-X-1305.

Cramer, M.S., 2012. "Numerical estimates for the bulk viscosity of ideal gases". *Physics of Fluids*, Vol. 24, No. 6, p. 066102. doi:10.1063/1.4729611.

Gillespie, L.J., 1930. "The Gibbs-Dalton law of partial pressures". *Physical Review*, Vol. 36, No. 1, p. 121.

Gnoffo, P.A., Gupta, R.N. and Shinn, J.L., 1989. "Conservation equations and physical models for hypersonic air flows in thermal and chemical nonequilibrium". Technical report, NASA Report 2867.

Hirsch, C., 2007. *Numerical Computation of Internal and External Flows: The Fundamentals of Computational Fluid Dynamics*. Elsevier, Oxford.

Jawahar, P. and Kamath, H., 2000. "A high-resolution procedure for Euler and Navier–Stokes computations on unstructured grids". *Journal of Computational Physics*, Vol. 164, No. 1, pp. 165–203. doi:10.1006/jcph.2000.6596.

Johnston, C.O., Hollis, B.R. and Sutton, K., 2008. "Nonequilibrium stagnation-line radiative heating for Fire II". *Journal of Spacecraft and Rockets*, Vol. 45, No. 6, pp. 1185–1195.

MacCormack, R.W. and Candler, G.V., 1989. "The solution of the Navier-Stokes equations using Gauss-Seidel line relaxation". *Computers & Fluids*, Vol. 17, No. 1, pp. 135–150. doi:10.1016/0045-7930(89)90012-1.

Martin, A., Scalabrin, L.C. and Boyd, I.D., 2012. "High performance modeling of atmospheric re-entry vehicles". *Journal of Physics: Conference Series*, Vol. 341, p. 012002. doi:10.1088/1742-6596/341/1/012002.

Moreira, F.C., Wolf, W.R. and Azevedo, J.L.F., 2021. "Thermal analysis of hypersonic flows of carbon dioxide and air in thermodynamic non-equilibrium". *International Journal of Heat and Mass Transfer*, Vol. 165, p. 120670. doi: 10.1016/j.ijheatmasstransfer.2020.120670.

Niu, Q., Yuan, Z., Dong, S. and Tan, H., 2018. "Assessment of nonequilibrium air-chemistry models on species formation in hypersonic shock layer". *International Journal of Heat and Mass Transfer*, Vol. 127, pp. 703–716. ISSN 0017-9310. doi:https://doi.org/10.1016/j.ijheatmasstransfer.2018.07.007.

Nompelis, I., Candler, G. and Conti, R., 2009. "A parallel implicit CFD code for the simulation of ablating re-entry vehicles". In AIAA Paper No. 2009-1562*, 47th AIAA Aerospace Sciences Meeting*. Orlando, FL. doi:10.2514/6.2009-1562.

Park, C., 1988. "Assessment of a two-temperature kinetic model for dissociating and weakly ionizing nitrogen". *Journal of Thermophysics and Heat Transfer*, Vol. 2, No. 1, pp. 8–16. doi:10.2514/3.55.

Park, C., 1989. "Assessment of two-temperature kinetic model for ionizing air". *Journal of Thermophysics and Heat Transfer*, Vol. 3, No. 3, pp. 233–244. doi:10.2514/3.28771.

Park, C., 1993. "Review of chemical-kinetic problems of future NASA missions. i-Earth entries". *Journal of Thermophysics and Heat Transfer*, Vol. 7, No. 3, pp. 385–398. doi:10.2514/3.431.

Scalabrin, L.C., 2007. *Numerical Simulation of Weakly Ionized Hypersonic Flow over Reentry Capsules*. Ph.D. thesis, University of Michigan.

Sharma, B. and Kumar, R., 2019. "Estimation of bulk viscosity of dilute gases using a nonequilibrium molecular dynamics approach". *Phys. Rev. E*, Vol. 100, p. 013309. doi:10.1103/PhysRevE.100.013309.

Steger, J.L. and Warming, R., 1981. "Flux vector splitting of the inviscid gasdynamic equations with application to finite-difference methods". *Journal of Computational Physics*, Vol. 40, No. 2, pp. 263–293. doi:10.1016/0021-9991(81)90210-2.

Venkatakrishnan, V., 1995. "Implicit schemes and parallel computing in unstructured grid CFD". Technical report, NASA CR-195071.

Vincenti, W. and Kruger, C., 1982. *Introduction to Physical Gas Dynamics*. Wiley.

Wilke, C.R., 1950. "A viscosity equation for gas mixtures". *The Journal of Chemical Physics*, Vol. 18, No. 4, pp. 517–519. doi:10.1063/1.1747673.

8. RESPONSIBILITY NOTICE

The authors are solely responsible for the printed material included in this paper.